Free vibration analysis of circular plates with multiple circular holes using indirect BIEMs

Wei-Ming Lee[a], Jeng-Tzong Chen[b] and Ying-Te Lee[b]

[a] Department of Mechanical Engineering, China Institute of Technology, Taipei, Taiwan

wmlee@cc.chit.edu.tw

[b] Department of Harbor and River Engineering, National Taiwan Ocean University, Keelung, Taiwan

Abstract

In this paper, a semi-analytical approach is proposed to solve natural frequencies and natural modes for circular plates with multiple circular holes by using the indirect formulation in conjunction with degenerate kernels and Fourier series. All the kernels in the indirect formulation are expanded into degenerate form. By uniformly collocating points on the boundary, a linear algebraic system can be constructed. The direct searching approach is adopted to determine the natural frequency through singular value decomposition (SVD). After determining the unknown Fourier coefficients, the corresponding mode shape is obtained by using the indirect boundary integral formulations. The results of the annular plate, as a special case, are compared with the analytical solution to verify the validity of the present method. For the cases of circular plates with multiple circular holes, the results are also compared with those of finite element method (FEM) using ABAQUS. Good accuracy, high rate of convergence and computational efficiency are the main features of the present method due to the semi-analytical procedure.

Keywords: semi-analytical approach, boundary integral formulation, plate problem, biharmonic equation, circular hole, degenerate kernel

1. Introduction

Circular plates with multiple circular holes are widely used in engineering structures [1], e.g. missiles, aircraft, etc., either to reduce the weight of the whole structure or to increase the range of inspection. These holes in the structure usually cause the change of natural frequency as well as the decrease of the corresponding strength. The comprehension of the associated effects is helpful to the work of mechanical design and flight control of the structure. As quoted by Leissa [2], the free vibrations of circular plates have been of practical and academic interest for at least a century and a half. Although the results for circular or annular plates are available in the literature [1,2,3,4,5,6,7,8]; however, all of these publications except [1,6,8] are confined to plates with concentric hole. Although a large amount of papers on the circular membrane vibration with circular holes were published [9], very a few papers on the free vibration of plate with several holes can be found. Vibration analysis of annular-like plates were solved by using FEM [1, 8] to study the effect of eccentricity more than 1500 elements [8] are required. To propose a semi-analytical approach for solving the circular plate with circular holes is not trivial and is the main goal of this research.

In the past, some analytical solutions [3] for natural frequencies of the circular or annular plates were obtained. Frequency equations are obtained by substituting the general solution, satisfied the governing equation of plates, into the boundary conditions. These analytic solutions were confirmed experimentally but some analytic solutions corresponding to the clamped boundary condition showed little derivation from the experimental results due to the lack of stiffness of the clamped

boundary condition in reality. Since an analytical solution of natural frequencies requires the solution of special functions (e.g. Bessel function and modified Bessel function), Vera *et al.* [4] obtained analytical solutions by implementing the same procedure as [3] in the Maple V system and pointed out some inaccurate results in [2]. Regarding to the circular plate with multiple holes, the analytical solution of the natural frequencies and the corresponding mode shapes have not so far been solved due to the fourth-order partial differential equation and complex geometry configurations.

In the other hand, diverse numerical methods were resorted to the solution of plate problems, which include finite difference method (FDM), finite element method (FEM) and boundary element method (BEM). BEM has some advantages in comparison with domain discretization methods (FEM, FDM). The main gain is that the boundary element method reduces the dimension of the original problem by one, thus, the number of the introduced unknowns is much less than that of the traditional domain type methods. In addition, the domain mesh generation is not required, which is generally the most difficult and time consuming task. For the BEM applications to plate problems, readers may consult with the review article [10]. It is noted that improper integrals on the boundary should be handled particularly when the BEM is used. In the past, many researchers proposed several regularization techniques to deal with the singularity and hypersingularity. To determine the Cauchy principal value (CPV) and the Hadamard principal value (HPV) in the singular and hypersingular integrals is a critical issue in BEM/BIEM [11,12]. For the plate problem, it is more difficult to calculate the principle values since the kernels are involved with transcendental complex functions. Based on direct boundary integral formulation, Chen *et al.* [6,13] recently proposed null-field integral equations in conjunction with degenerate kernels and Fourier series to solve boundary value problems with circular boundaries. Some applications were done in the static stress calculations of anti-plane and plate problems. For the indirect BEM, Ventsel [14] has solved the static plate problems. In this paper, we utilize degenerate kernels and Fourier series to solve the plate eigenproblem. The degenerate kernel can be derived by expanding the fundamental solution into a series form on each side of the circular boundary by employing the addition theorem. In reality, addition theorems are expansion formulae for the special functions (e.g. Bessel function, Legendre functions, spherical harmonics, etc.) in a selected coordinate system [15]. Therefore, degenerate kernel, namely separable kernel and Fourier series, are vital tools to study the circular plate with circular holes.

The purpose of this paper is to propose a semi-analytical approach to solve the natural frequencies and natural modes of circular plate with multiple circular holes by using the indirect boundary integral formulation in conjunction with degenerate kernels and Fourier series. The indirect formulation by choosing the single-layer and double-layer potential is proposed and the fictitious density distribution on the boundary is represented by using Fourier series in the adaptive coordinate system. A linear algebraic system is constructed by uniformly locating the collocation points on the boundary. By matching the boundary conditions, the determinant of the matrix must be zero to obtain the nontrivial eigensolution. The direct searching approach [16] is adopted to determine the natural frequency by using singular value decomposition (SVD). After determining the Fourier coefficients, the corresponding mode shape of the circular plate with multiple circular holes can be obtained by using the indirect boundary integral equations. For the plate problem in the polar coordinate system, the slope (bending angle), moment and effective shear force in the normal and tangential directions for the non-concentric domain must be determined with care. Therefore, the technique of vector and tensor transformation is adopted to deal with the problem for the non-concentric plate. Finally, The

analysis result of the annular plate, as our special case, is compared with the analytical solution [2,3,4] to verify the validity of the present method. The results of the circular plate with eccentric circular hole and multiple circular holes are compared with those of Khurasia and Rawtani [1] and FEM using ABAQUS to demonstrate the generality of the proposed method.

2. Problem statement and indirect boundary integral formulation

2.1 Problem statement of plate eigenproblem

The governing equation for the free flexural vibration of a uniform thin plate with randomly distributed circular holes as shown in Figure 1 is written as follows:

$$\nabla^4 u(x) = \lambda^4 u(x), \qquad x \in \Omega, \tag{1}$$

where u is the lateral displacement, $\lambda^4 = \omega^2 \rho_0 h/D$, λ is the frequency parameter, ω is the circular frequency, ρ_0 is the volume density, D is the flexural rigidity expressed as $D = Eh^3/12(1-\nu^2)$ in terms of the Young's modulus E, the Poisson ratio ν and the plate thickness h, and Ω is the domain of the thin plate.

2.2 Indirect boundary integral formulation

The kernel function $U(s,x)$ is the fundamental solution which satisfies

$$\nabla^4 U(s,x) - \lambda^4 U(s,x) = \delta(s-x), \tag{2}$$

where ∇^4 is the biharmonic operator, $\delta(s-x)$ is the Dirac-delta function, and s and x are the source and field points, respectively. Considering the two singular solutions ($Y_0(\lambda r)$ and $K_0(\lambda r)$, which are the zeroth-order of the second-kind Bessel and modified Bessel functions, respectively) and two regular solutions ($J_0(\lambda r)$ and $I_0(\lambda r)$, which are the zeroth-order of the first-kind Bessel and modified Bessel functions, respectively) in the fundamental solution, we have

$$U(s,x) = \frac{1}{8\lambda^2}[Y_0(\lambda r) + iJ_0(\lambda r) + \frac{2}{\pi}(K_0(\lambda r) + iI_0(\lambda r))] \tag{3}$$

where $r \equiv |s-x|$ and $i^2 = -1$.

Based on the indirect boundary integral formulation, the displacement field of plate vibration can be represented by

$$u(x) = \int_B P(s,x)\phi(s)dB(s) + \int_B Q(s,x)\varphi(s)dB(s), \tag{4}$$

where $P(s,x)$ and $Q(s,x)$ are any two of the four kernel functions (U, Θ, M and V) which will be elaborated on later; $\phi(s)$ and $\psi(s)$ are the unknown fictitious density distributions on the boundary. $U(s,x)$ is the fundamental solution in Eq.(3) and the other three kernels, $\Theta(s,x)$, $M(s,x)$ and $V(s,x)$, can be obtained by applying the following operators defined by

$$K_\Theta(\cdot) = \frac{\partial(\cdot)}{\partial n} \tag{5}$$

$$K_M(\cdot) = \nu\nabla^2(\cdot) + (1-\nu)\frac{\partial^2(\cdot)}{\partial n^2} \tag{6}$$

$$K_V(\cdot) = \frac{\partial}{\partial n}\nabla^2(\cdot) + (1-\nu)\frac{\partial}{\partial t}[\frac{\partial}{\partial n}(\frac{\partial}{\partial t}(\cdot))] \tag{7}$$

to the kernel $U(s,x)$ with respect to the source point, where $\frac{\partial}{\partial n}$ and $\frac{\partial}{\partial t}$ are the normal and tangential derivatives, respectively. Since the kernels $P(s,x)$ and $Q(s,x)$ can be selected from any two of the four kernels, $U(s,x)$, $\Theta(s,x)$, $M(s,x)$ and $V(s,x)$, six (C_2^4) formulations can be considered. For simplicity, the kernels $U(s,x)$ and $\Theta(s,x)$ are chosen as $P(s,x)$ and $Q(s,x)$ in Eq.(4). In addition to the displacement, the slope, normal moment and effective shear force can be derived by applying the three operators in Eqs.(5), (6) and (7) to Eq.(4) with respect to the field point. Then, the indirect boundary integral representations of the displacement, slop, moment and effect shear force are expressed as follows:

$$u(x) = \int_B U(s,x)\phi(s)dB(s) + \int_B \Theta(s,x)\varphi(s)dB(s) \tag{8}$$

$$\theta(x) = \int_B U_\theta(s,x)\phi(s)dB(s) + \int_B \Theta_\theta(s,x)\varphi(s)dB(s) \tag{9}$$

$$m(x) = \int_B U_m(s,x)\phi(s)dB(s) + \int_B \Theta_m(s,x)\varphi(s)dB(s) \tag{10}$$

$$v(x)=\int_B U_v(s,x)\phi(s)dB(s)+\int_B \Theta_v(s,x)\varphi(s)dB(s) \qquad (11)$$

For the clamped case, the lateral displacement $u(x)$ and the slope $\theta(x)$ on the boundary are specified to zero. For the free case, the normal moment $m(x)$ and effective shear force $v(x)$ on the boundary are set to zero.

2.3 Degenerate kernels and Fourier series for the fictitious boundary densities

In the polar coordinate, the field point and source point can be expressed as (ρ,ϕ) and (R,θ), respectively. By employing the separation technique for the source and field points, the kernel function $U(s,x)$ is expanded in the series form as follows:

$$\begin{aligned} U^I(s,x)=&\frac{1}{8\lambda^2}\sum_{m=0}^{\infty}\varepsilon_m\{J_m(\lambda\rho)[Y_m(\lambda R)+iJ_m(\lambda R)] \\ &+\frac{2}{\pi}I_m(\lambda\rho)[K_m(\lambda R)+i(-1)^m I_m(\lambda R)]\} \\ &\cos[m(\theta-\varphi)], \qquad \rho<R, \end{aligned} \qquad (12)$$

$$\begin{aligned} U^E(s,x)=&\frac{1}{8\lambda^2}\sum_{m=0}^{\infty}\varepsilon_m\{J_m(\lambda R)[Y_m(\lambda\rho)+iJ_m(\lambda\rho)] \\ &+\frac{2}{\pi}I_m(\lambda R)[K_m(\lambda\rho)+i(-1)^m I_m(\lambda\rho)]\} \\ &\cos[m(\theta-\varphi)], \qquad \rho\geq R, \end{aligned} \qquad (13)$$

where ε_m is the Neumann factor (ε_m =1, m=0 ; ε_m =2, m=1,2, … ,∞) and the superscripts "*I*" and "*E*" denote the interior and exterior cases for $U(s,x)$ degenerate kernel to distinguish $r<R$ and $r>R$, respectively. The other degenerate kernels $\Theta(s,x)$, $U_\theta(s,x)$, $\Theta_\theta(s,x)$, $U_m(s,x)$, $\Theta_m(s,x)$, $U_v(s,x)$ and $\Theta_v(s,x)$ in the indirect boundary integral equations can be obtained by applying the operators of Eqs.(5)-(7) to the degenerate kernel $U(s,x)$ in Eqs.(12) and (13) with respect to the field point *x* or source point *s*.

In order to fully utilize the geometry of circular boundary, the fictitious boundary densities, $\phi(s)$ and $\psi(s)$, can be expanded by employing the Fourier series. Therefore we obtain

$$\phi(s)=a_0+\sum_{m=0}^{\infty}(a_m\cos m\theta+b_m\sin m\theta),\ \mathrm{s}\in\mathrm{B} \qquad (14)$$

$$\psi(s)=p_0+\sum_{m=0}^{\infty}(p_m\cos m\theta+p_m\sin m\theta),\ \mathrm{s}\in\mathrm{B} \qquad (15)$$

where a_0 , a_m , b_m , p_0 , p_m and q_m are the Fourier coefficients and θ is the polar angle. In the real computation, only the finite *M* terms are used in the summation of Eqs. (14) and (15).

3. Adaptive observer system and transformation of tensor components

3.1 Adaptive observer system

Consider a plate problem with circular boundaries as shown in Figure 1. Since the indirect boundary integral equations are frame indifferent (*i.e.* rule of objectivity), the origin of the observer system can be adaptively located on the center of the corresponding boundary contour under integration. Adaptive observer system is chosen to fully employ the circular property by expanding the kernels into degenerate forms. Figure 2 shows the boundary integration for the circular boundaries in the adaptive observer system. The dummy variable in the circular contour integration is the angle (θ) instead of radial coordinate (*R*). By using the adaptive system, all the boundary integrals can be determined analytically free of principal value senses.

3.2 Transformation of tensor components

Since the calculation of the slope, moment and effective shear force are involved in the plate problem, potential gradient or higher-order gradient is required to calculate carefully. For the non-concentric case, special treatment for the potential gradient should be taken care as the source and field points locate on different circular boundaries. As shown in Figure 3, the angle ϕ_i of the collocation point x_i is described in the center of the circle under integration and the angle ϕ_c is described in the center of the circle on which collocation point is located. According to the transformation of the component of the vector Eq.(16) and the tensor Eq.(17), we have

$$\begin{bmatrix}(\cdot)_n\\(\cdot)_t\end{bmatrix}=\begin{bmatrix}cos(\delta) & sin(\delta)\\ -sin(\delta) & cos(\delta)\end{bmatrix}\begin{bmatrix}(\cdot)_r\\(\cdot)_\theta\end{bmatrix} \tag{16}$$

$$\begin{bmatrix}(\cdot)_{nn}\\(\cdot)_{nt}\end{bmatrix}=\begin{bmatrix}\cos^2(\delta) & sin^2(\delta) & 2\sin(\delta)\cos(\delta)\\ -\sin(\delta)\cos(\delta) & \sin(\delta)\cos(\delta) & \cos^2(\delta)-sin^2(\delta)\end{bmatrix}\begin{bmatrix}(\cdot)_r\\(\cdot)_\theta\\(\cdot)_{r\theta}\end{bmatrix} \tag{17}$$

The three operators in Eqs.(5)-(7) can be transformed as follows:

$$K_\theta^R=\cos(\delta)\frac{\partial(\cdot)}{\partial n}+\sin(\delta)\frac{\partial(\cdot)}{\partial t} \tag{18}$$

$$K_M^R=[\nu+(1-\nu)\sin^2(\delta)]\nabla^2(\cdot)+\cos(2\delta)(1-\nu)\frac{\partial^2(\cdot)}{\partial n^2}+\sin(2\delta)(1-\nu)\frac{\partial}{\partial n}\left(\frac{\partial(\cdot)}{\partial t}\right) \tag{19}$$

$$K_V^R=\cos(\delta)\frac{\partial}{\partial n}\nabla^2(\cdot)+\sin(\delta)[1+(1-\nu)\cos(\delta)]\frac{\partial}{\partial t}\nabla^2(\cdot)-\sin(2\delta)(1-\nu)\frac{\partial}{\partial t}\left(\frac{\partial^2(\cdot)}{\partial n^2}\right)+\cos(2\delta)(1-\nu)\frac{\partial}{\partial t}\left[\frac{\partial}{\partial n}\left(\frac{\partial(\cdot)}{\partial t}\right)\right] \tag{20}$$

where $\delta=\phi_c-\phi_i$. When the angle ϕ_c equals to the angle ϕ_i or the angle difference δ equals to zero, Eqs. (18)-(20) are simplified to the Eqs.(5)-(7). Considering non-concentric cases, the degenerate kernels, $U_\theta(s,x)$, $\Theta_\theta(s,x)$, $U_m(s,x)$, $\Theta_m(s,x)$, $U_\nu(s,x)$ and $\Theta_\nu(s,x)$, can be obtained by applying the operators of Eqs.(18)-(20) to the degenerate kernel $U(s,x)$ and $\Theta(s,x)$ with respect to the field point *x*.

4. Linear algebraic system

Consider the plate problem with circular domain containing *H* randomly distributed circular holes centered at the position vector $\boldsymbol{c}_j$ ($j=1,2,3,\cdots,L$), (*L*= 1+ *H* and $\boldsymbol{c}_1$ is the position vector of the outer circular boundary for the plate), as shown in Figure 4 in which R_j denotes the radius of the *j*th circular region and B_j is the boundary of the *j*th circular hole. By uniformly collocating the *N* (=2*M*+1) points on each circular boundary in Eqs.(8)-(11), we have

$$u(x)=\sum_{j=1}^{L}\int_{B_j}\{U(s,x)\phi(s)+\Theta(s,x)\psi(s)\}dB_j(s),\quad x\in\Omega \tag{21}$$

$$\theta(x)=\sum_{j=1}^{L}\int_{B_j}\{U_\theta(s,x)\phi(s)+\Theta_\theta(s,x)\psi(s)\}dB_j(s),\quad x\in\Omega \tag{22}$$

$$m(x)=\sum_{j=1}^{L}\int_{B_j}\{U_m(s,x)\phi(s)+\Theta_m(s,x)\psi(s)\}dB_j(s),\quad x\in\Omega \tag{23}$$

$$v(x)=\sum_{j=1}^{L}\int_{B_j}\{U_\nu(s,x)\phi(s)+\Theta_\nu(s,x)\psi(s)\}dB_j(s).\quad x\in\Omega \tag{24}$$

The main gain by using degenerate kernel is that singular integrals can be easily determined. The selection of interior or exterior degenerate kernel depends on $\rho<R$ or $\rho>R$, respectively, according to the observer system. For the B_j integral of circular boundary, the degenerate kernels of $U(s,x)$, $\Theta(s,x)$, $U_\theta(s,x)$, $\Theta_\theta(s,x)$, $U_m(s,x)$, $\Theta_m(s,x)$, $U_\nu(s,x)$ and $\Theta_\nu(s,x)$ are utilized while the fictitious boundary density $\phi(s)$ and $\psi(s)$ along the circular boundary are substituted by using the Fourier series of Eqs.(14) and (15), respectively. In the B_j integration, the origin of the observer system is adaptively set to collocate at the center c_j to utilize the degenerate kernels and Fourier series. By considering the outer circular boundary clamped and inner circular boundary free as an example, a linear algebraic system can be written due to orthogonal property as follows:

$$\begin{bmatrix}U^{11} & \Theta^{11} & U^{12} & \Theta^{12} & \cdots & U^{1L} & \Theta^{1L}\\ U_\theta^{11} & \Theta_\theta^{11} & U_\theta^{12} & \Theta_\theta^{12} & \cdots & U_\theta^{1L} & \Theta_\theta^{1L}\\ U_m^{21} & \Theta_m^{21} & U_m^{22} & \Theta_m^{22} & \cdots & U_m^{2L} & \Theta_m^{2L}\\ U_\nu^{21} & \Theta_\nu^{21} & U_\nu^{22} & \Theta_\nu^{22} & \cdots & U_\nu^{2L} & \Theta_\nu^{2L}\\ \vdots & \vdots & \vdots & \vdots & \ddots & \vdots & \vdots\\ U_m^{L1} & \Theta_m^{L1} & U_m^{L2} & \Theta_m^{L2} & \cdots & U_m^{LL} & \Theta_m^{LL}\\ U_\nu^{L1} & \Theta_\nu^{L1} & U_\nu^{L2} & \Theta_\nu^{L2} & \cdots & U_\nu^{LL} & \Theta_\nu^{LL}\end{bmatrix}\begin{Bmatrix}\Phi^1\\ \Psi^1\\ \Phi^2\\ \Psi^2\\ \vdots\\ \Phi^L\\ \Psi^L\end{Bmatrix}=\begin{Bmatrix}0\\0\\0\\0\\\vdots\\0\\0\end{Bmatrix}, \tag{25}$$

where *L* denotes the number of circular boundaries (including inner and outer circular boundaries). For brevity, a unified form [U^{ij}] ($i=1,2,3,\cdots,L$ and $j=1,2,3,\cdots,L$) denote the response of $U(s,x)$ kernel at the *i*th circle point due to the source at the *j*th circle. Otherwise, the same definition is for [Θ^{ij}], [U_θ^{ij}], [Θ_θ^{ij}], [U_m^{ij}], [Θ_m^{ij}], [U_ν^{ij}] and [Θ_ν^{ij}] kernels. The sub-vectors [Φ^i] and [Ψ^i] and the sub-matrices of [U^{ij}],[Θ^{ij}], [U_θ^{ij}], [Θ_θ^{ij}], [U_m^{ij}], [Θ_m^{ij}],[U_ν^{ij}] and [Θ_ν^{ij}] are defined as follows:

$$\boldsymbol{\Phi}^i = \begin{Bmatrix} a_0^i \\ a_1^i \\ b_1^i \\ \vdots \\ a_M^i \\ b_M^i \end{Bmatrix} \qquad \boldsymbol{\Psi}^i = \begin{Bmatrix} p_0^i \\ p_1^i \\ q_1^i \\ \vdots \\ p_M^i \\ q_M^i \end{Bmatrix} \tag{26}$$

$$U^{ij} = \begin{bmatrix} U_{0C}^{ij}(\rho_1,\phi_1) & U_{1C}^{ij}(\rho_1,\phi_1) & U_{1S}^{ij}(\rho_1,\phi_1) & \cdots & U_{MS}^{ij}(\rho_1,\phi_1) \\ U_{0C}^{ij}(\rho_2,\phi_2) & U_{1C}^{ij}(\rho_2,\phi_2) & U_{1S}^{ij}(\rho_2,\phi_2) & \cdots & U_{MS}^{ij}(\rho_2,\phi_2) \\ \vdots & \vdots & \vdots & & \vdots \\ \vdots & \vdots & \vdots & & \vdots \\ U_{0C}^{ij}(\rho_N,\phi_N) & U_{1C}^{ij}(\rho_N,\phi_N) & U_{1S}^{ij}(\rho_N,\phi_N) & \cdots & U_{MS}^{ij}(\rho_N,\phi_N) \end{bmatrix}_{N\times N} \tag{27}$$

$$\Theta^{ij} = \begin{bmatrix} \Theta_{0C}^{ij}(\rho_1,\phi_1) & \Theta_{1C}^{ij}(\rho_1,\phi_1) & \Theta_{1S}^{ij}(\rho_1,\phi_1) & \cdots & \Theta_{MS}^{ij}(\rho_1,\phi_1) \\ \Theta_{0C}^{ij}(\rho_2,\phi_2) & \Theta_{1C}^{ij}(\rho_2,\phi_2) & \Theta_{1S}^{ij}(\rho_2,\phi_2) & \cdots & \Theta_{MS}^{ij}(\rho_2,\phi_2) \\ \vdots & \vdots & \vdots & & \vdots \\ \vdots & \vdots & \vdots & & \vdots \\ \Theta_{0C}^{ij}(\rho_N,\phi_N) & \Theta_{1C}^{ij}(\rho_N,\phi_N) & \Theta_{1S}^{ij}(\rho_N,\phi_N) & \cdots & \Theta_{MS}^{ij}(\rho_N,\phi_N) \end{bmatrix}_{N\times N} \tag{28}$$

$$U_\theta^{ij} = \begin{bmatrix} U_{\theta,0C}^{ij}(\rho_1,\phi_1) & U_{\theta,1C}^{ij}(\rho_1,\phi_1) & U_{\theta,1S}^{ij}(\rho_1,\phi_1) & \cdots & U_{\theta,MS}^{ij}(\rho_1,\phi_1) \\ U_{\theta,0C}^{ij}(\rho_2,\phi_2) & U_{\theta,1C}^{ij}(\rho_2,\phi_2) & U_{\theta,1S}^{ij}(\rho_2,\phi_2) & \cdots & U_{\theta,MS}^{ij}(\rho_2,\phi_2) \\ \vdots & \vdots & \vdots & & \vdots \\ \vdots & \vdots & \vdots & & \vdots \\ U_{\theta,0C}^{ij}(\rho_N,\phi_N) & U_{\theta,1C}^{ij}(\rho_N,\phi_N) & U_{\theta,1S}^{ij}(\rho_N,\phi_N) & \cdots & U_{\theta,MS}^{ij}(\rho_N,\phi_N) \end{bmatrix}_{N\times N} \tag{29}$$

$$\Theta_\theta^{ij} = \begin{bmatrix} \Theta_{\theta,0C}^{ij}(\rho_1,\phi_1) & \Theta_{\theta,1C}^{ij}(\rho_1,\phi_1) & \Theta_{\theta,1S}^{ij}(\rho_1,\phi_1) & \cdots & \Theta_{\theta,MS}^{ij}(\rho_1,\phi_1) \\ \Theta_{\theta,0C}^{ij}(\rho_2,\phi_2) & \Theta_{\theta,1C}^{ij}(\rho_2,\phi_2) & \Theta_{\theta,1S}^{ij}(\rho_2,\phi_2) & \cdots & \Theta_{\theta,MS}^{ij}(\rho_2,\phi_2) \\ \vdots & \vdots & \vdots & & \vdots \\ \vdots & \vdots & \vdots & & \vdots \\ \Theta_{\theta,0C}^{ij}(\rho_N,\phi_N) & \Theta_{\theta,1C}^{ij}(\rho_N,\phi_N) & \Theta_{\theta,1S}^{ij}(\rho_N,\phi_N) & \cdots & \Theta_{\theta,MS}^{ij}(\rho_N,\phi_N) \end{bmatrix}_{N\times N} \tag{30}$$

$$U_m^{ij} = \begin{bmatrix} U_{m,0C}^{ij}(\rho_1,\phi_1) & U_{m,1C}^{ij}(\rho_1,\phi_1) & U_{m,1S}^{ij}(\rho_1,\phi_1) & \cdots & U_{m,MS}^{ij}(\rho_1,\phi_1) \\ U_{m,0C}^{ij}(\rho_2,\phi_2) & U_{m,1C}^{ij}(\rho_2,\phi_2) & U_{m,1S}^{ij}(\rho_2,\phi_2) & \cdots & U_{m,MS}^{ij}(\rho_2,\phi_2) \\ \vdots & \vdots & \vdots & & \vdots \\ \vdots & \vdots & \vdots & & \vdots \\ U_{m,0C}^{ij}(\rho_N,\phi_N) & U_{m,1C}^{ij}(\rho_N,\phi_N) & U_{m,1S}^{ij}(\rho_N,\phi_N) & \cdots & U_{m,MS}^{ij}(\rho_N,\phi_N) \end{bmatrix}_{N\times N} \tag{31}$$

$$\Theta_m^{ij} = \begin{bmatrix} \Theta_{m,0C}^{ij}(\rho_1,\phi_1) & \Theta_{m,1C}^{ij}(\rho_1,\phi_1) & \Theta_{m,1S}^{ij}(\rho_1,\phi_1) & \cdots & \Theta_{m,MS}^{ij}(\rho_1,\phi_1) \\ \Theta_{m,0C}^{ij}(\rho_2,\phi_2) & \Theta_{m,1C}^{ij}(\rho_2,\phi_2) & \Theta_{m,1S}^{ij}(\rho_2,\phi_2) & \cdots & \Theta_{m,MS}^{ij}(\rho_2,\phi_2) \\ \vdots & \vdots & \vdots & & \vdots \\ \vdots & \vdots & \vdots & & \vdots \\ \Theta_{m,0C}^{ij}(\rho_N,\phi_N) & \Theta_{m,1C}^{ij}(\rho_N,\phi_N) & \Theta_{m,1S}^{ij}(\rho_N,\phi_N) & \cdots & \Theta_{m,MS}^{ij}(\rho_N,\phi_N) \end{bmatrix}_{N\times N} \tag{32}$$

$$U_\nu^{ij} = \begin{bmatrix} U_{\nu,0C}^{ij}(\rho_1,\phi_1) & U_{\nu,1C}^{ij}(\rho_1,\phi_1) & U_{\nu,1S}^{ij}(\rho_1,\phi_1) & \cdots & U_{\nu,MS}^{ij}(\rho_1,\phi_1) \\ U_{\nu,0C}^{ij}(\rho_2,\phi_2) & U_{\nu,1C}^{ij}(\rho_2,\phi_2) & U_{\nu,1S}^{ij}(\rho_2,\phi_2) & \cdots & U_{\nu,MS}^{ij}(\rho_2,\phi_2) \\ \vdots & \vdots & \vdots & & \vdots \\ \vdots & \vdots & \vdots & & \vdots \\ U_{\nu,0C}^{ij}(\rho_N,\phi_N) & U_{\nu,1C}^{ij}(\rho_N,\phi_N) & U_{\nu,1S}^{ij}(\rho_N,\phi_N) & \cdots & U_{\nu,MS}^{ij}(\rho_N,\phi_N) \end{bmatrix}_{N\times N} \tag{33}$$

$$\Theta_\nu^{ij} = \begin{bmatrix} \Theta_{\nu,0C}^{ij}(\rho_1,\phi_1) & \Theta_{\nu,1C}^{ij}(\rho_1,\phi_1) & \Theta_{\nu,1S}^{ij}(\rho_1,\phi_1) & \cdots & \Theta_{\nu,MS}^{ij}(\rho_1,\phi_1) \\ \Theta_{\nu,0C}^{ij}(\rho_2,\phi_2) & \Theta_{\nu,1C}^{ij}(\rho_2,\phi_2) & \Theta_{\nu,1S}^{ij}(\rho_2,\phi_2) & \cdots & \Theta_{\nu,MS}^{ij}(\rho_2,\phi_2) \\ \vdots & \vdots & \vdots & & \vdots \\ \vdots & \vdots & \vdots & & \vdots \\ \Theta_{\nu,0C}^{ij}(\rho_N,\phi_N) & \Theta_{\nu,1C}^{ij}(\rho_N,\phi_N) & \Theta_{\nu,1S}^{ij}(\rho_N,\phi_N) & \cdots & \Theta_{\nu,MS}^{ij}(\rho_N,\phi_N) \end{bmatrix}_{N\times N} \tag{34}$$

where ϕ_k and ρ_k ($k = 1,2,3,\cdots,N$) are the kth collocation angle and radius of the collocation point on each boundary in the observer system and the element of the sub-matrices are defined as follows:

$$U_{nC}^{ij}(\rho_i,\phi_i) = \int_0^{2\pi} U(R,\theta;\rho_i,\phi_i)\cos(n\theta)(Rd\theta) \qquad n=0,1,2,\cdots,M, \tag{35}$$

$$U_{nS}^{ij}(\rho_i,\phi_i) = \int_0^{2\pi} U(R,\theta;\rho_i,\phi_i)\sin(n\theta)(Rd\theta) \qquad n=1,2,\cdots,M, \tag{36}$$

$$\Theta_{nC}^{ij}(\rho_i,\phi_i) = \int_0^{2\pi} \Theta(R,\theta;\rho_i,\phi_i)\cos(n\theta)(Rd\theta) \qquad n=0,1,2,\cdots,M, \tag{37}$$

$$\Theta_{nS}^{ij}(\rho_i,\phi_i) = \int_0^{2\pi} \Theta(R,\theta;\rho_i,\phi_i)\sin(n\theta)(Rd\theta) \qquad n=1,2,\cdots,M, \tag{38}$$

$$U_{\theta,nC}^{ij}(\rho_i,\phi_i) = \int_0^{2\pi} U_\theta(R,\theta;\rho_i,\phi_i)\cos(n\theta)(Rd\theta) \qquad n=0,1,2,\cdots,M, \tag{39}$$

$$U_{\theta,nS}^{ij}(\rho_i,\phi_i) = \int_0^{2\pi} U_\theta(R,\theta;\rho_i,\phi_i)\sin(n\theta)(Rd\theta) \qquad n=1,2,\cdots,M, \tag{40}$$

$$\Theta_{\theta,nC}^{ij}(\rho_i,\phi_i) = \int_0^{2\pi} \Theta_\theta(R,\theta;\rho_i,\phi_i)\cos(n\theta)(Rd\theta) \qquad n=0,1,2,\cdots,M, \tag{41}$$

$$\Theta_{\theta,nS}^{ij}(\rho_i,\phi_i) = \int_0^{2\pi} \Theta_\theta(R,\theta;\rho_i,\phi_i)\sin(n\theta)(Rd\theta) \qquad n=1,2,\cdots,M, \tag{42}$$

$$U_{m,nC}^{ij}(\rho_i,\phi_i) = \int_0^{2\pi} U_m(R,\theta;\rho_i,\phi_i)\cos(n\theta)(Rd\theta) \qquad n=0,1,2,\cdots,M, \tag{43}$$

$$U_{m,nS}^{ij}(\rho_i,\phi_i) = \int_0^{2\pi} U_m(R,\theta;\rho_i,\phi_i)\sin(n\theta)(Rd\theta) \qquad n=1,2,\cdots,M, \tag{44}$$

$$\Theta_{m,nC}^{ij}(\rho_i,\phi_i) = \int_0^{2\pi} \Theta_m(R,\theta;\rho_i,\phi_i)\cos(n\theta)(Rd\theta) \qquad n=0,1,2,\cdots,M, \tag{45}$$

$$\Theta_{m,nS}^{ij}(\rho_i,\phi_i) = \int_0^{2\pi} \Theta_m(R,\theta;\rho_i,\phi_i)\sin(n\theta)(Rd\theta) \qquad n=1,2,\cdots,M, \tag{46}$$

$$U_{\nu,nC}^{ij}(\rho_i,\varphi_i) = \int_0^{2\pi} U_\nu(R,\theta;\rho_i,\varphi_i)\cos(n\theta)(Rd\theta) \qquad n=0,1,2,\cdots,M, \tag{47}$$

$$U_{\nu,nS}^{ij}(\rho_i,\varphi_i) = \int_0^{2\pi} U_\nu(R,\theta;\rho_i,\varphi_i)\sin(n\theta)(Rd\theta) \qquad n=1,2,\cdots,M, \tag{48}$$

$$\Theta_{\nu,nC}^{ij}(\rho_i,\phi_i) = \int_0^{2\pi} \Theta_\nu(R,\theta;\rho_i,\phi_i)\cos(n\theta)(Rd\theta) \qquad n=0,1,2,\cdots,M, \tag{49}$$

$$\Theta_{\nu,nS}^{ij}(\rho_i,\phi_i) = \int_0^{2\pi} \Theta_\nu(R,\theta;\rho_i,\phi_i)\sin(n\theta)(Rd\theta) \qquad n=1,2,\cdots,M, \tag{50}$$

where the interior degenerate kernels are used for $j=1$, $i=1,2,3,\cdots,N$; otherwise, exterior degenerate kernels are used. According to the direct-searching scheme, the eigenvalues can be obtained by applying the SVD technique to the matrix in the left hand of Eq.(25). Once the eigenvalues are obtained, the associated mode shape can be obtained by substituting the corresponding eigenvectors (i.e. the Fourier series representing the fictitious boundary density) into the indirect boundary integral representation. The procedure of solution is described in a flowchart as shown in Figure 5.

5. Numerical results and discussions

Case1: *A circular plate with an eccentric hole* [1]

A circular plate weakened by an eccentric hole is considered. The offset distance *e* of the eccentric hole is 0.45m (e/a=0.45) as shown in Figure 6. The former six natural frequency parameters using different numbers of terms of Fourier series (*M*) are shown in Figure 7. It shows that the number of terms used influences the natural frequency parameter as well as the number of mode. Since the induced eccentric hole affects the characteristics symmetry, some diametric nodes, e.g. the second, the fourth and the sixth modes, are lost when insufficient terms of Furrier series are used. Figure 8 indicates the minimum singular value of the influence matrix versus the

frequency parameter λ using seven terms of Fourier series (M=7). The multiplicity is one only due to the asymmetry. The FEM model of the ABAQUS used 8217 elements and 8404 nodes. The former six natural frequency parameters and modes by using FEM [1] and the present method are shown in Figure 9. The results of the present method match well with those of FEM using ABAQUS. In the results of Khurasia and Rawtani [1], the first mode was not reported while the second and fourth modes are lost. A little deviation is also shown in the results reported by Khurasia and Rawtani due to the coarse mesh. Owing to the lack of stiffness of the clamped boundary condition in reality, it is expected that the experimental data [1] are less than those obtained by the other methods.

Case2: *A circular plate with two holes*

In order to demonstrate the generality of the present method, a circular plate with two holes is considered as shown in Figure 10. The radii of holes are 0.25m and 0.15m and the coordinates of the center are (0.5,0) and (-0.4,-0.3), respectively, in the coordinate system with origin at the center of outer circle. The former five natural frequency parameters using different numbers of terms of Fourier series (M) is shown in Figure 11. Owning to the complex configuration, the fewer terms of Fourier series (M=*1* or *2*) can not approach the second and higher natural frequencies of parameters well. Figure 12 shows the minimum singular value of the influence matrix versus the frequency parameter λ where the number of Fourier series terms M is taken as 7. Figure 13 shows the former five natural frequency parameters and modes of FEM using ABAQUS and the present method. Good agreement between the results of the present method and those of ABAQUS is obtained.

6. Concluding remarks

A semi-analytical approach for solving the natural frequencies and natural modes for the circular plate with multiple circular holes was proposed. Instead of employing the direct formulation, the present method used indirect boundary integral equations in conjugation with the degenerate kernels and the Fourier series to represent the fictitious boundary densities in the adaptive observer system. The improper integrals in the indirect BIEs were avoided by employing the degenerate kernels and were easily calculated through the series sum. The potential across the circular boundary was described explicitly from the interior and exterior expressions of degenerate kernels. The degenerate kernels of the slope, moment and effective shear force in the plate eigenproblems have been derived. Once the Fourier coefficients of fictitious boundary densities have been determined, the corresponding mode shape can be obtained by using the indirect boundary integral representation. The natural frequencies and corresponding mode shapes for the multiply-connected plate problems with circular boundaries and multiple circular holes have been solved easily and efficiently by using the present method in comparison with the available exact solutions and FEM results using ABAQUS.

References

[1] H. B. Khurasia and S. Rawtani, “Vibration analysis of circular plates with eccentric hole,” *ASME Journal of Applied Mechanics,* vol. 45, pp. 215-217, 1978.

[2] A. W. Leissa, *Vibration of plates*, NASA SP-160; 1969.

[3] S. M. Vogel and D. W. Skinner, “Natural frequencies of transversely vibrating uniform annular plates,” *ASME Journal of Applied Mechanics*, vol. 32, pp. 926-931, 1965.

[4] D. A. Vega, S. A. Vera, M. D. Sa Â Nchez and P. A. A. Laura, “Transverse vibrations of circular, annular plates with a free inner boundary,” *Journal of the Acoustical Society of America*, vol. 103, pp. 1225-1226, 1998.

[5] J. T. Chen, S. Y. Lin, I. L. Chen and Y. T. Lee, “Mathematical analysis and numerical study to free vibrations of annular plates using BIEM and BEM,”

International Journal for Numerical Methods in Engineering, vol. 65, pp. 236–263, 2006.

[6] J. T. Chen, C. C. Hsiao and S. Y. Leu, "Null-field integral equation approach for plate problems with circular holes," *ASME Journal of Applied Mechanics*, in press (2006).

[7] J. T. Chen, Y. T. Lee, I. L. Chen and K. H. Chen, "Mathematical analysis and treatment for the true and spurious eigenequations of circular plates by the meshless method using radial basis function," *Journal of the Chinese Institute of Engineers*, vol. 27(4), pp. 547-561, 2004.

[8] L. Cheng, Y. Y. Li and L. H. Yam, "Vibration analysis of annular-like plates," *Journal of Sound and Vibration*, vol. 262, pp. 1153-1170, 2003.

[9] K. Nagaya and K. Poltorak, "Method for solving eigenvalue problems of the Helmholtz equation with a circular outer and a number of eccentric circular inner boundaries," *Journal of the Acoustical Society of America*, vol. 85, pp. 576-581, 1989.

[10] C. P. Providatis and D. E. Beskos, "Dynamic analysis of plates by boundary elements," *ASME Applied Mechanics Reviews*, vol. 52(7), pp. 213-236, 1999.

[11] M. Tanaka, V. Sladek and J. Sladek, "Regularization techniques applied to boundary element methods," *Applied Mechanics Reviews*, vol. 47, pp. 457-499, 1994.

[12] J. T. Chen and H.-K. Hong, "Review of dual boundary element methods with emphasis on hypersingular integrals and divergent series," *ASME Applied Mechanics Reviews*, vol. 52(1), pp. 17-33, 1999.

[13] J. T. Chen, W. C. Shen and A. C. Wu, "Null-field integral equations for stress field around circular holes under anti-plane shear," *Engineering Analysis with Boundary Elements*, vol. 30, pp. 205-217, 2006.

[14] E. S. Ventsel, "An indirect boundary element method for plate bending analysis," *International Journal for Numerical Methods in Engineering*, vol. 40, pp. 1597-1610, 1997.

[15] I. S. Gradshteyn and I. M. Ryzhik, *Table of integrals, series, and products*, 5th edition, Academic Press; 1996.

[16] M. Kitahara, *Boundary Integral Equation Methods in Eigenvalue Problems of Elastodynamics and Thin Plates*, Elsevier: Amsterdam; 1985.

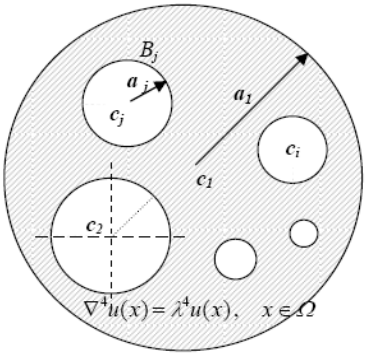

Figure 1. Problem statement for an eigenproblem with multiple circular holes

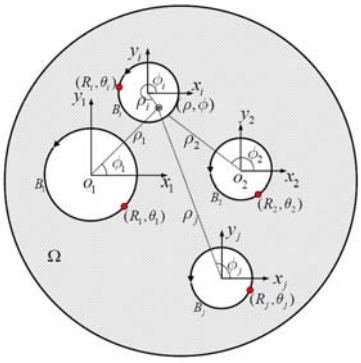

Figure 2. Adaptive observer system when integrating the corresponding circular boundaries

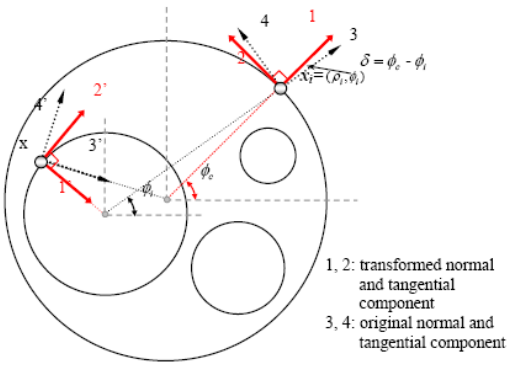

Figure 3. Transformation of tensor components

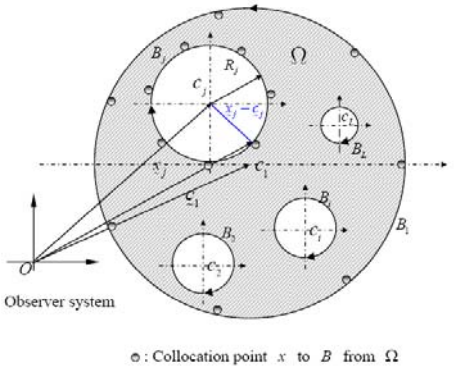

Figure 4. Collocation point and boundary contour integration in the boundary integral equation

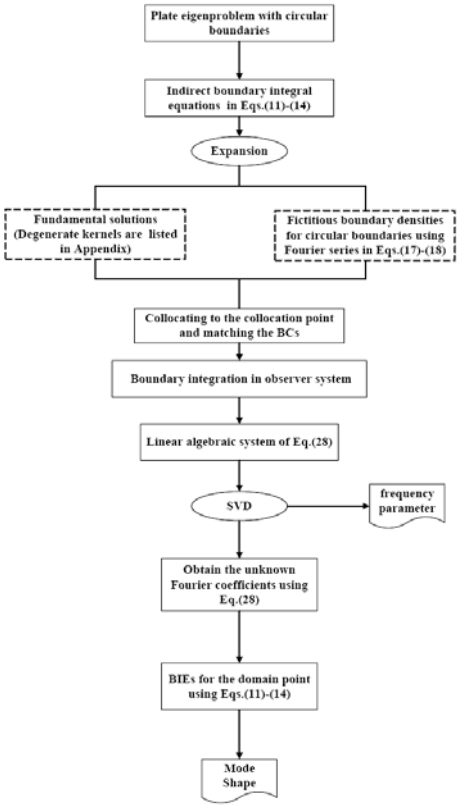

Figure 5. Flowchart of the present method

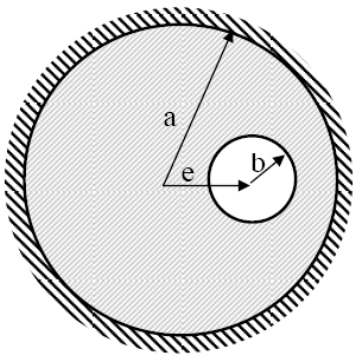

Geometric data:
a=1m
b=0.25m
e=0.45m
Boundary condition:
Inner circle : free
Outer circle: clamped

Figure 6. A circular plate with an eccentric hole in clamped-free boundary condition

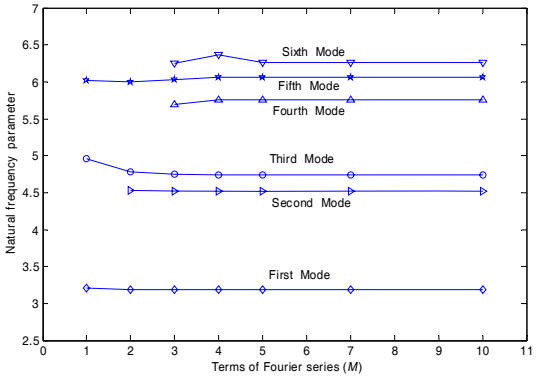

Figure 7. Natural frequency parameter versus terms of Fourier series for a circular plate with an eccentric hole

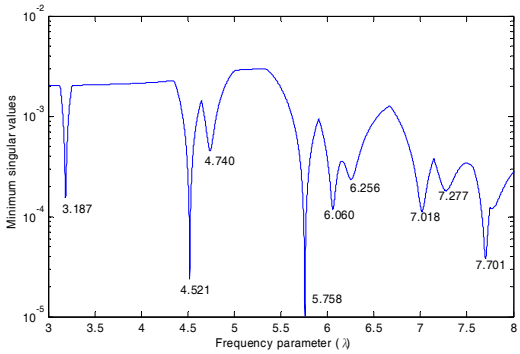

Figure 8. The minimum singular value versus the frequency parameter for a circular plate with one eccentric hole

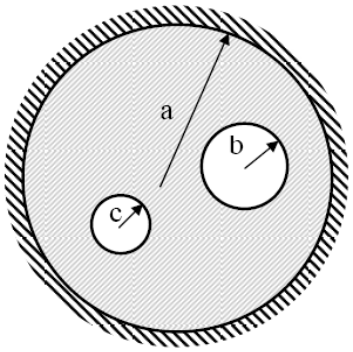

Case3:

Geometric data:
a=1m
b=0.25m
c=0.125m
Boundary condition:
Inner circle : free
Outer circle: clamped

Figure 10. A circular plate with two circular holes in clamped-free boundary condition

MODE	1	2	3	4	5	6
Present method	3.1870	4.5210	4.7400	5.7580	6.0600	6.2560
	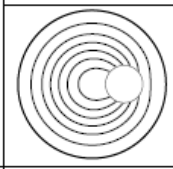	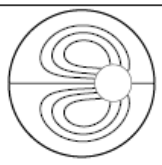	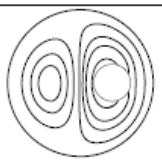	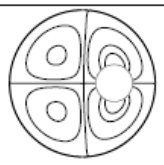	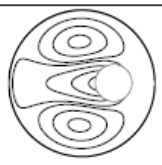	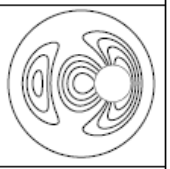
ABAQUS	3.2020	4.5300	4.7450	5.7753	6.0899	6.2361
	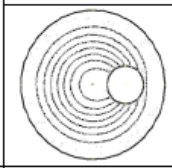	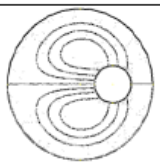	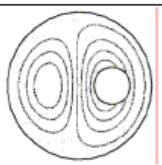	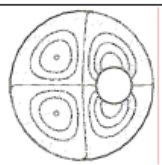	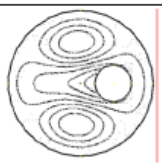	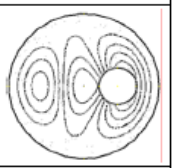
Khurasia and Rawtani [1]	3.1623	N/A	4.6690	N/A	5.8138	6.0828
	<2.8810>	N/A	<4.6904>	N/A	<5.6391>	N/A
	N/A	N/A	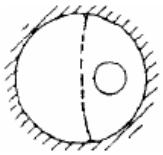	N/A	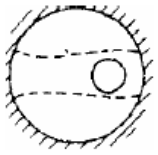	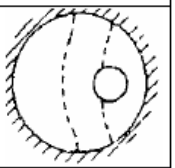

Figure 9. The former six natural frequency parameters and modes of a circular plate with an eccentric hole

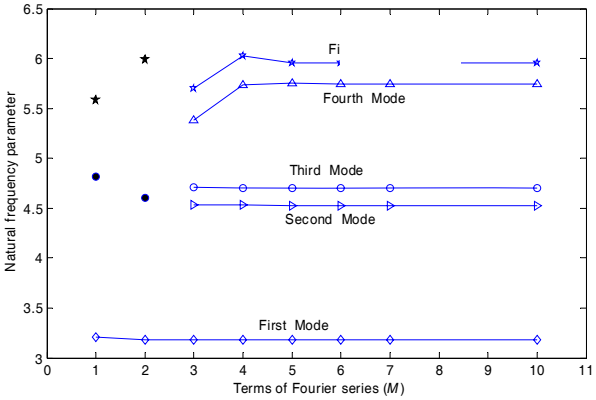

Figure 11. Natural frequency parameter versus terms of Fourier series for a circular plate with two holes

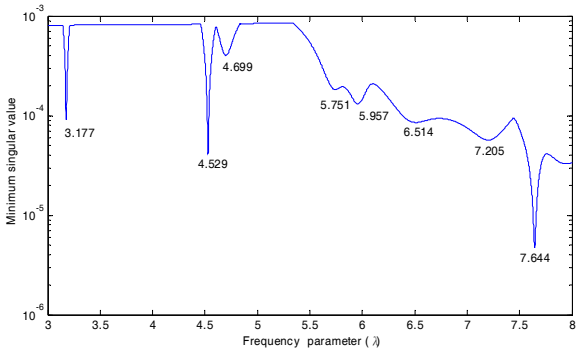

Figure 12. The minimum singular value versus the frequency parameter for a circular plate with two holes

MODE	1	2	3	4	5
Present method	3.1770	4.5290	4.699	5.7510	5.9570
	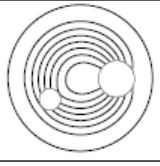	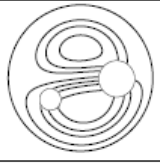			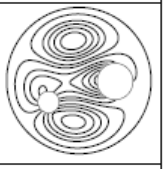
ABAQUS	3.1950	4.5296	4.7086	5.8070	6.0280
	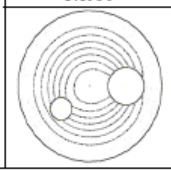	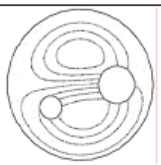			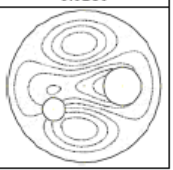

Figure 13. The former five eigenvalues and eigenmodes of a circular plate with two holes